




Research Article

Regulation on Calcium Oxalate Crystallization and Protection on HK-2 Cells of Tea Polysaccharides with Different Molecular Weights

Hong Liu ¹, Xin-Yuan Sun ², Feng-Xin Wang,¹ and Jian-Ming Ouyang ¹

¹Department of Chemistry, Institute of Biomineralization and Lithiasis Research, Jinan University, Guangzhou 510632, China

²Department of Urology, Guangzhou Institute of Urology, Guangdong Key Laboratory of Urology, The First Affiliated Hospital of Guangzhou Medical University, Guangzhou Medical University, Guangzhou, Guangdong 510230, China

Correspondence should be addressed to Jian-Ming Ouyang; toyjm@jnu.edu.cn

Received 20 January 2020; Accepted 15 April 2020; Published 13 May 2020

Guest Editor: German Gil

Copyright © 2020 Hong Liu et al. This is an open access article distributed under the Creative Commons Attribution License, which permits unrestricted use, distribution, and reproduction in any medium, provided the original work is properly cited.

The regulation on calcium oxalate (CaOx) crystallization and protective effect on human proximal tubular epithelial cells (HK-2) of four green tea polysaccharides (TPSs) with molecular weights of 10.88 (TPS0), 8.16 (TPS1), 4.82 (TPS2), and 2.3 kDa (TPS3) were comparatively studied. XRD, Fourier transform infrared spectroscopy, and scanning electron microscopy results revealed that TPS1, TPS2, and TPS3 can increase the percentage of the dihydrate crystalline phase in CaOx crystals and reduce the size of CaOx monohydrate crystals. TPSs increased the absolute value of the zeta potential of CaOx crystal and inhibited crystal nucleation and aggregation. The nucleation inhibition rates of TPS1, TPS2, and TPS3 to CaOx crystallization were 56.67%, 75.52%, and 52.92%, respectively, and their aggregation inhibition rates were 22.34%, 47.59%, and 21.59%, respectively. TPS preprotection can alleviate the oxidative damage of HK-2 cells caused by oxalate, increase cell viability, protect cell morphology, and reduce lactate dehydrogenase release and reactive oxygen species levels. The degraded TSPs, especially TPS2 with moderate molecular weight, may be used as a green drug to inhibit stone formation.

1. Introduction

Kidney stone is one of the most common diseases, and its main components are calcium oxalate (CaOx) monohydrate (COM) and CaOx dihydrate (COD) [1], and COM is more common than COD [2]. Stone formation is generally dependent on the level of imbalance between the urinary inhibitors and promoters of crystallization [3]. Many stone inhibitors, such as organic macromolecular glycosaminoglycans, citric acid, and phosphate, are present in urine [4, 5].

In patients with kidney stones, oxalate and CaOx crystals induce the generation of free radicals in renal epithelial cells, which generate oxidative stress, thereby leading to the formation of kidney stones [6]. Plant polysaccharides not only can reduce cell oxidative damage by scavenging free radicals [7]

but also can inhibit the nucleation, aggregation, and growth of crystals [8, 9]. The biological activity of plant polysaccharides is related to the physicochemical properties of the polysaccharide, such as the molecular weight of polysaccharides and acidic groups in polysaccharides [10]. Shi et al. [11] showed that the degraded polysaccharide with a low molecular weight (44 kDa) from *Enteromorpha prolifera* has a stronger antioxidant capacity than crude polysaccharide from *E. prolifera* (1400 kDa). In vivo, low-molecular-weight polysaccharides have better protective effects on oxalate-induced oxidative damage than high-molecular-weight heparin and fucoidan [12, 13].

Tea is one of the most extensive drinks in the world, especially in Asia. Tea polysaccharide (TPS) is one of the most important components in tea. Although many studies have

been conducted on TPSs, most of them focused on pharmacological properties, which include anti-inflammatory, anticancer, antioxidation, hypocholesterolemic, blood pressure lowering, and other biological activities [14–16], and the research on inhibiting CaOx kidney stones are few.

In our previous study [17], we used H_2O_2 to degrade the original TPS (TPS0) with a molecular weight of 10.88 kDa and obtained three degraded polysaccharides with molecular weights of 8.16 (TPS1), 4.82 (TPS2), and 2.31 (TPS3) kDa, and their structures were characterized. TPSs have an antioxidant effect and repair effect on damaged human renal proximal tubular cells (HK-2). After TPS repair, the damage of COM to HK-2 cells can be effectively reduced, and the adhesion of COM crystals to cells can be reduced [18].

In this study, we studied the regulation of TPSs on CaOx crystallization and the ability of TPSs to protect renal epithelial cells from oxidative damage to develop new green, natural antistone drugs.

2. Materials and Methods

2.1. Materials and Apparatus

2.1.1. Materials. Green tea polysaccharide (TPS) was purchased from Shaanxi Ciyuan Biological Co., Ltd. Three different molecular weights of degraded polysaccharides TPS1, TPS2, and TPS3 were obtained by H_2O_2 oxidative degradation according to Reference [16]. The molecular weight and carboxyl ($-COOH$) content of TPSs are shown in Table 1. Human proximal tubular epithelial cells (HK-2) were purchased from Shanghai cell bank of the Chinese Academy of Sciences (Shanghai, China).

The cell proliferation assay kit (CCK-8), lactate dehydrogenase (LDH) kit, hematoxylin and eosin (HE) staining kit, and reactive oxygen species assay kit (DCFH-DA) were from Shanghai Beyotime Bio-Tech Co., Ltd., Shanghai, China. Fetal bovine serum and cell culture medium (DMEM) were from Gibco, USA. Penicillin and streptomycin were from Beijing Pubo Biotechnology Co., Ltd., Beijing, China. Cell culture plates of 6, 12, and 96 well were from NEST, China. Anhydrous calcium chloride ($CaCl_2$), sodium oxalate (Na_2Ox), and the other conventional reagents were from Guangzhou chemical reagent factory, China.

2.1.2. Apparatus. Fourier transform infrared spectroscopy (FT-IR) was from EQUINOX55, Bruker, Germany. Ultraviolet-visible spectrophotometer was from Cary 500, Varian company, USA. The X-ray powder diffractometer (D/MAX2400) was from Japan. The X-L type environmental scanning electron microscope (ESEM) was from Philips, Eindhoven, Netherlands, and a Nano Measurer 1.2.5 Software (Fudan University, China) was used to determine the average size of the CaOx crystals from the SEM images. Inverted fluorescence microscope was from Olympus company, Japan. The optical microscope was from OlyMPUS, CKX41, Japan. The Zetasizer Nano ZS90 apparatus was from Malvern, England. The flow cytometer was from Beckman, Gallios, USA. The microplate reader was from SafireZ, Tecan, Switzerland.

TABLE 1: Carboxyl content of TPSs with different molecular weights and CaOx crystal phase difference induced by 0.1 g/L of TPS.

TPS	Molecular weight (kDa)	$-COOH$ content (%)	$c(TPS)$ (g/L)	COM content (%)	COD content (%)
Blank	0	—	0	100	0
TPS0	10.88	11.2	0.1	100	0
TPS1	8.16	12.3	0.1	27	73
TPS2	4.82	12.7	0.1	20	80
TPS3	2.31	11.0	0.1	69	31

2.2. Experimental Methods

2.2.1. Crystallization of CaOx. Experiments were carried out with slight modification according to Reference [19]. The reaction was maintained and conducted in a 100 mL beaker at $37^\circ C$. Firstly, 4.4 mg, 6.6 mg, 13.2 mg, 22.0 mg, and 35.2 mg of TPSs with different molecular weights were added to 22 mmol/L $CaCl_2$ solution (20 mL) and magnetically stirred for 10 min. Sodium oxalate (22 mmol/L, 20 mL) was then added to the mixture until the final volume of 44 mL was obtained. The final concentrations of both Ca^{2+} and Ox^{2-} were 10 mmol/L, and the polysaccharide concentrations were 0.1, 0.15, 0.3, 0.5, and 0.8 g/L. After stirring for 10 min, the mixture was maintained at $37^\circ C$ for 2 h, and the suspension was centrifuged to obtain CaOx deposits. The bottom deposits of CaOx were dried for component analysis through XRD and FT-IR, and some precipitates were ultrasonically dispersed with anhydrous alcohol to facilitate the morphological observation through scanning electron microscopy (SEM). The relative percentage contents of COM and COD in the CaOx precipitates were calculated through the K value method and according to the XRD patterns:

$$COD\% = \frac{I_{COD}}{I_{COD} + I_{COM}}, \quad (1)$$

where I_{COM} and I_{COD} are the intensity of the main diffraction peak ($\bar{1}01$) crystal plane of COM and the main diffraction peak (200) crystal plane of COD, respectively.

2.2.2. Zeta Potential Measurement of CaOx Crystals. CaOx crystals were dispersed in double distilled water with 200 $\mu g/mL$ concentration. After ultrasonication for 10 min, the zeta potential was detected with a Zetasizer Nano ZS90 apparatus at $25^\circ C$.

2.2.3. CaOx Crystallization Assay. The change in turbidity in the reaction system was detected with a UV spectrophotometer, and the inhibition effect of TPSs on the nucleation (S_N) and aggregation rates (S_A) of the CaOx crystals were studied [20]. CaOx crystallization was achieved by using a mixture of $CaCl_2$ solution (8 mmol/L) and sodium oxalate (1 mmol/L), containing 200 mmol/L NaCl, and 10 mmol/L NaAc and by adjusting the pH to 5.7.

A total of 1 mL of $CaCl_2$ solution (8 mmol/L) were stirred constantly at $37^\circ C$ in the absence or presence of TPSs

(0.1 g/L). Crystallization was induced by adding 1 mL of Na₂Ox solution (1 mmol/L) to reach final concentrations of 4 mmol/L CaCl₂ and 0.5 mmol/L Na₂Ox. The change in turbidity over 20 min was measured at 620 nm.

The following three parameters characterize the crystallization process [21]: first, crystal S_N, which is the maximum increase in optical density (OD) over time and mainly reflects the maximum rate of formation of new particles, thereby representing crystal nucleation; second, S_A, which is derived from the maximum decrease in OD [22]; and third, maximum time (t_{max}), at which the crystals can neither nucleate nor grow [23]. All three parameters are measurable in the crystallization process of CaOx.

The percentage inhibition was calculated from the nucleation and S_A, as follows: $[1 - (S_{NT}/S_{NC})] \times 100$ for the rate of nucleation and $[(1 - S_{AT}/S_{AC})] \times 100$ for the rate of aggregation, where S_{NT} and S_{AT} are the slopes in the presence of the TPSs, and S_{NC} and S_{AC} are the slopes of the control experiment.

2.2.4. Cell Culture. HK-2 cells were cultured in DMEM medium containing 10% fetal bovine serum in a 5% CO₂ humidified environment at 37°C. Upon reaching a monolayer of 80%–90% confluence, cells were gently blown after trypsinization to form a cell suspension for subsequent cell experiments.

2.2.5. Toxicity Detection of TPSs on HK-2 Cells. Cell suspension with a cell concentration of 1×10^5 cells/mL was inoculated per well in 96-well plates and incubated for 24 h. Afterward, the culture medium was removed, and 100 μL of 20, 60, and 100 μg/mL TPSs with various molecular weights was added, and each concentration was repeated in five parallel wells. After incubation for 24 h, CCK-8 was added to each well and incubated for 1.5 h. Absorbance (A) was measured at 450 nm according to the CCK-8 kit instruction. Cell viability was determined using the following equation:

$$\text{Cell viability}(\%) = \frac{A(\text{treatment group})}{A(\text{control group})} \times 100 \quad (2)$$

2.2.6. Protective Effect of TPSs on HK-2 Cells by CCK-8. Cell suspension with a cell concentration of 1×10^5 cells/mL was inoculated per well in 96-well plates and incubated for 24 h. The cells were divided into three groups: (1) the control group, where only serum-free DMEM culture medium was added; (2) the protection group, where serum-free medium containing TPSs with concentrations of 20, 40, 60, 80 and 100 μg/mL was added, and the culture medium was aspirated after 12 h. The cells were then treated with 2.8 mmol/L sodium oxalate dissolved in PBS and incubated for 3.5 h; and (3) the injured group, in which 2.8 mmol/L sodium oxalate dissolved in PBS was added and incubated for 3.5 h. The absorbance values were measured using the enzyme mark instrument at 450 nm to detect the protective capacity of TPSs.

2.2.7. Lactate Dehydrogenase (LDH) Release Assay. Cell suspension with a cell concentration of 1×10^5 cells/mL was inoculated per well in 96-well plates and incubated for 24 h. The cells were divided into three groups: (1) the control group, where only serum-free DMEM culture medium was added; (2) protection group, where serum-free medium containing TPSs with concentrations 80 μg/mL was added, and the culture medium was aspirated after 12 h; then, the cells were treated with 2.8 mmol/L sodium oxalate dissolved in PBS and incubated for 3.5 h; and (3) the injured group, in which 2.8 mmol/L sodium oxalate dissolved in PBS was added and incubated for 3.5 h. LDH release was measured with a microplate reader in accordance with the LDH kit test instructions. Absorbance was measured at 490 nm with a reference wavelength of 620 nm.

2.2.8. Cell Morphology Observation by Hematoxylin-Eosin (HE) Staining. The density of seeded cells and experimental grouping was the same as those in Section 2.2.7. After the treatment time was reached, the supernatant was then removed by aspiration and the cells were washed twice with PBS. Cells were fixed with 4% paraformaldehyde for 15 min and stained with hematoxylin and eosin according to the manufacturer's instructions. Morphological changes of the cells were observed under a microscope.

2.2.9. Changes in Intracellular Reactive Oxygen Species (ROS) Levels. The density of seeded cells and experimental grouping was the same as those in Section 2.2.7. After the treatment time was reached, 500 μL DCFH-DA diluted with serum-free culture medium at 1:1000 was added and incubated for 30 min at 37°C. ROS distribution was observed under a fluorescent microscope; the fluorescence intensity of intracellular ROS was quantitatively detected by flow cytometer.

2.2.10. Statistical Analysis. Experimental data were expressed as the mean ± standard deviation ($\bar{x} \pm SD$). The experimental results were analyzed statistically using SPSS 13.0 software (SPSS Inc., Chicago, IL, USA). The differences in the means between the experimental groups and the control group were analyzed using one-way ANOVA, followed by the Tukey post hoc test. If $p < 0.05$, there was significant difference; if $p < 0.01$, the difference was extremely significant; and if $p > 0.05$, there was no significant difference.

3. Results

3.1. Degraded TPSs Induce COD Formation. Figure 1(a) showed the XRD spectra of CaOx crystals induced by TPSs with different molecular weights. The diffraction peaks that appeared at the spacing d of 0.591, 0.364, 0.296, and 0.235 nm were attributed to the (101), (020), (202), and (130) crystal planes of COM, respectively. The diffraction peaks at d of 0.617, 0.441, 0.277, and 0.224 nm were attributed to the (200), (211), (411), and (213) planes of COD, respectively. Figure 1(a) shows that TPS with different molecular weights induced COD formation in different proportions (Table 1). For example, when TPS concentration was 0.1 g/L, the percentages of TPS-induced COD crystals followed the order of TPS2 (80%) > TPS1 (73%) > TPS3

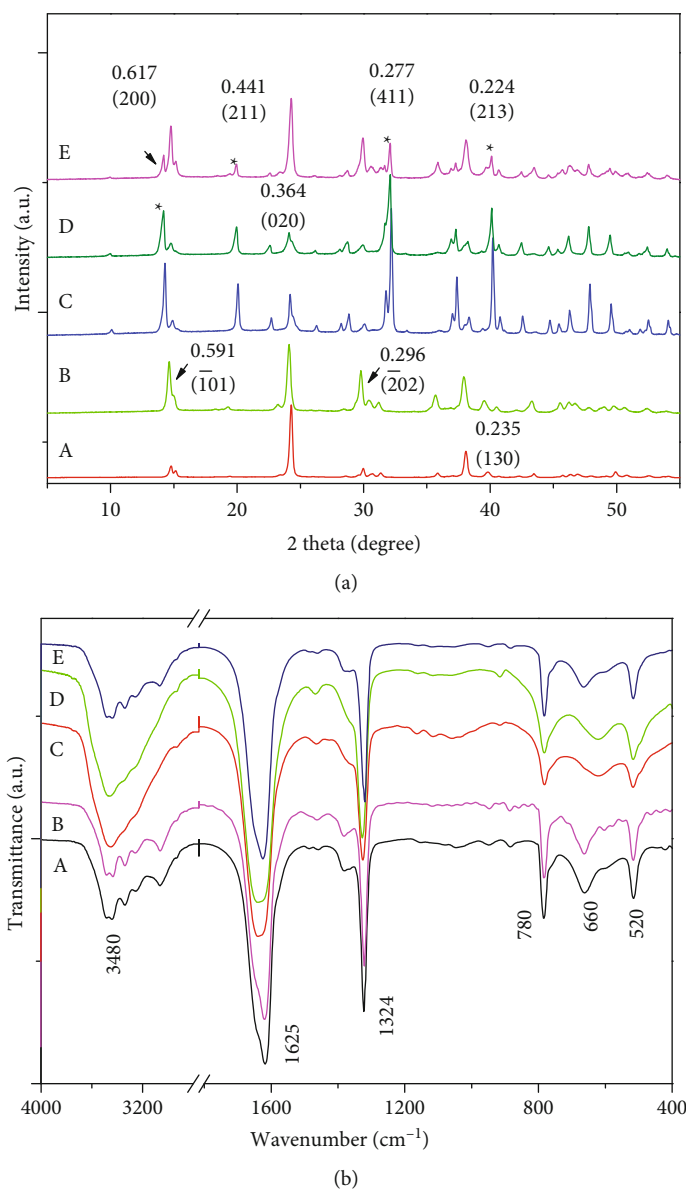


FIGURE 1: XRD patterns (a) and FT-IR spectra (b) of CaOx crystals induced by TPSs with different molecular weights. (A) Blank. (B) TPS0. (C)TPS1. (D) TPS2. (E) TPS3. $c(\text{Ca}^{2+}) = c(\text{Ox}^{2-}) = 10 \text{ mmol/L}$; $c(\text{TPS})$: 0.1 g/L; crystallization time: 2 h; * represents the main diffraction peaks of COD. The absence of * represents the main diffraction peaks of COM.

(31%)>TPS0 (0%); that is, TPS2 with moderate molecular weight had the highest induced COD content.

FT-IR spectra further confirmed XRD results. As shown in Figure 1(b), the FT-IR spectra of the CaOx crystals of the blank group, TPS0 (0.1 g/L), and TPS3 (0.1 g/L) were mainly the characteristic peaks of COM; that is, the formed crystals were mainly COM. However, in the presence of TPS1 (0.1 g/L) and TPS2 (0.1 g/L), the characteristic peaks of COD were the main peaks; that is, the formed crystals were mainly COD.

For COM crystals, a set of stretching vibration peaks was composed of five peaks at 3485–3047 cm^{-1} (Figure 1(b)), which belong to the O–H bond of the COM crystals. However, COD only has a single broad absorption peak in this region (Figure 1(b)) [24]. The appearances of the asymmetri-

cal stretching $\nu_{\text{as}}(\text{COO}^-)$ and symmetrical stretching $\nu_{\text{s}}(\text{COO}^-)$ were near 1621 and 1325 cm^{-1} , respectively, which indicated the presence of the COM crystals. However, the occurrence of $\nu_{\text{as}}(\text{COO}^-)$ and $\nu_{\text{s}}(\text{COO}^-)$ at approximately 1647 and 1326 cm^{-1} [25], respectively, indicated the presence of the COD crystals. In the fingerprint region, the absorption band of the COM crystals appeared at approximately 947, 885, 780, and 663 cm^{-1} , while COD appeared at approximately 916 and 618 cm^{-1} .

3.2. Effect of TPSs with Different Concentrations on COD Formation. The XRD spectra of CaOx crystals induced by TPSs at different concentrations are shown in Figure 2. With the increase in TPS concentration, the diffraction peak of COD increased, thereby indicating that the percentage of

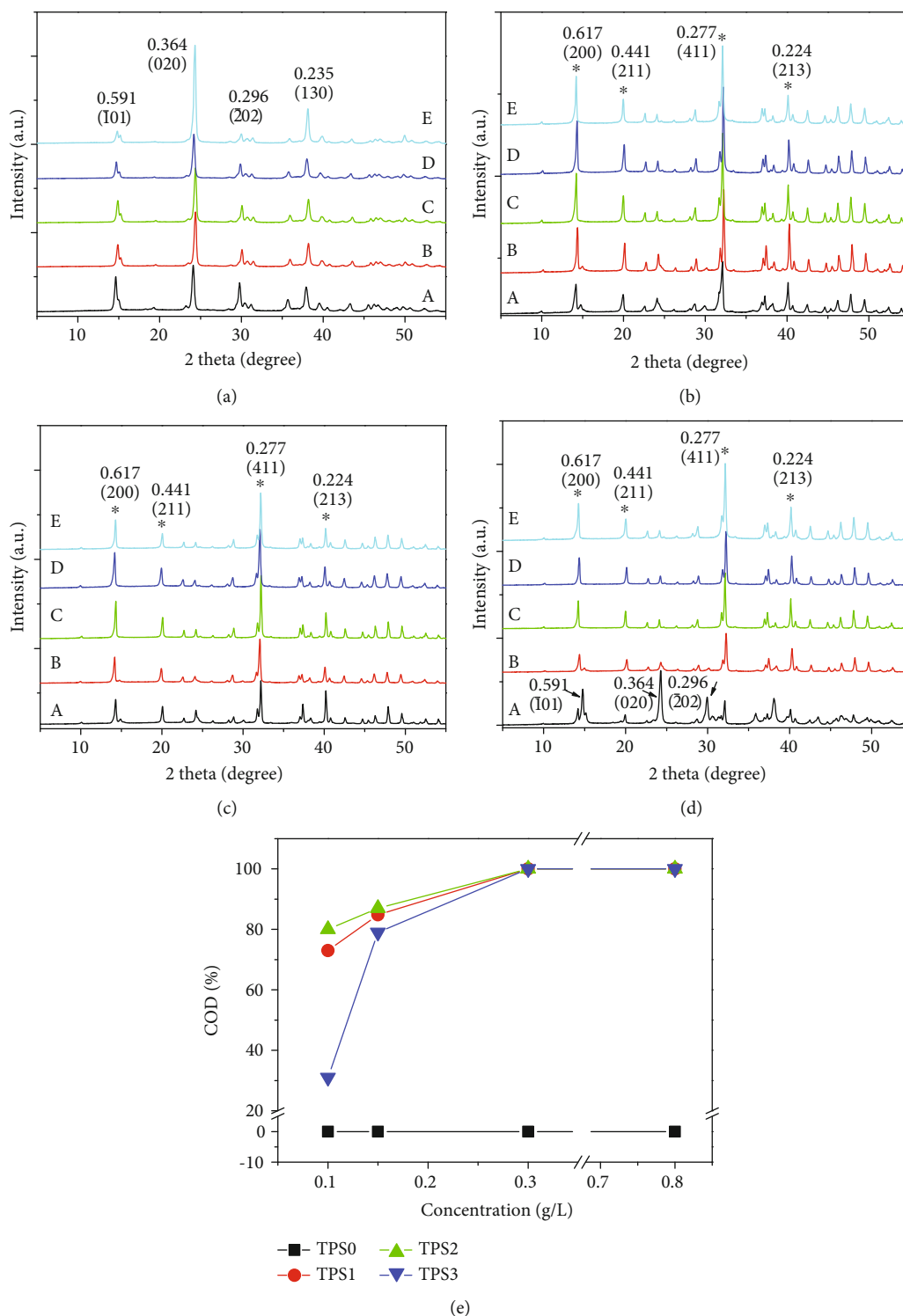


FIGURE 2: XRD patterns of CaOx crystals and COD content induced by different concentrations of TPSs. (a) TPS0. (b) TPS1. (c) TPS2. (d) TPS3. (e) Percentage of COD. $c(\text{TPS})$: (A) 0, (B) 0.1, (C) 0.15, (D) 0.3, (E) 0.8 g/L. $c(\text{Ca}^{2+}) = c(\text{Ox}^{2-}) = 10 \text{ mmol/L}$; crystallization time: 2 h.

induced COD increased. TPS1, TPS2, and TPS3 induced 100% COD at concentration of 0.3 g/L (Figure 2(e)). However, when the TPS0 concentration with the largest molecular weight was 0.8 g/L, the diffraction peak of COD was still not evident.

Figure 3 shows the FT-IR spectrum of the CaOx crystals induced by TPSs with different concentrations. With the increase in the TPS concentration from 0.1 g/L to 0.8 g/L, the $\nu_{\text{as}}(\text{COO}^-)$ and $\nu_{\text{s}}(\text{COO}^-)$ of the CaOx crystals underwent blue shifts at different degrees. For example, the ν_{as}

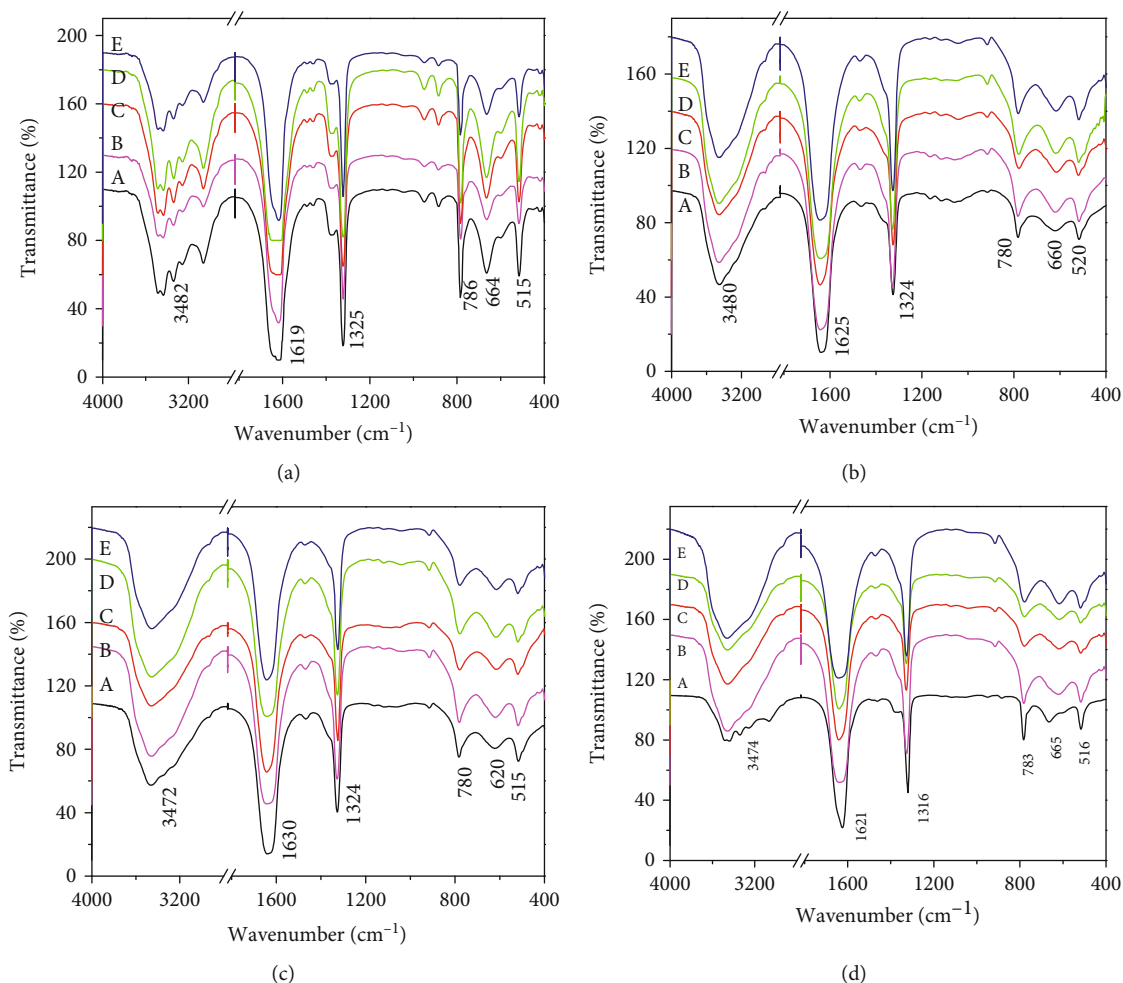


FIGURE 3: FT-IR spectra of CaOx crystals induced by different concentrations of TPSs. (a) TPS0. (b) TPS1. (c) TPS2. (d) TPS3. $c(\text{TPS})$: (A) 0, (B) 0.1, (C) 0.15, (D) 0.3, and (E) 0.8 g/L.

(COO⁻) in the crystals regulated by TPS2 increased from 1639 cm^{-1} to 1651 cm^{-1} , and $\nu_s(\text{COO}^-)$ increased from 1323 cm^{-1} to 1342 cm^{-1} (Table 2). The results showed that the COM percentage gradually decreased, while COD gradually increased.

3.3. SEM Observation of CaOx Crystals Regulated by TPSs.

Figure 4 shows the SEM images of the CaOx crystals induced by four TPSs at the concentration of 0.1 g/L. In the absence of polysaccharide, the formed crystals were COM crystals with irregular morphology and serious aggregation. After TPS0 was added, COM crystals were still obtained, but the crystal size was smaller than that of the control group. In the presence of 0.1 g/L TPS1 and TPS2, COD with blunt edges and corners were mainly formed, but the crystal size of the TPS2-regulated COD was small. TPS3-induced crystals had larger sizes, and the percentage of COD significantly decreased, and the degree of COM aggregation was also higher than that in TPS1 or TPS2.

In order to better quantify the difference in the particle size between different groups, we used Nano Measurer 1.2.5 Software (Fudan University, China) to determine the average

size of the CaOx crystals from the SEM images. This size was a statistical result of the average data from 100 single particles. The average particle sizes of the crystals in the blank group and four TPS treatment groups are $1.81 \pm 0.21\ \mu\text{m}$, $1.02 \pm 0.16\ \mu\text{m}$ (TPS0), $1.18 \pm 0.28\ \mu\text{m}$ (TPS1), $0.88 \pm 0.15\ \mu\text{m}$ (TPS2), and $2.64 \pm 0.84\ \mu\text{m}$ (TPS3), respectively.

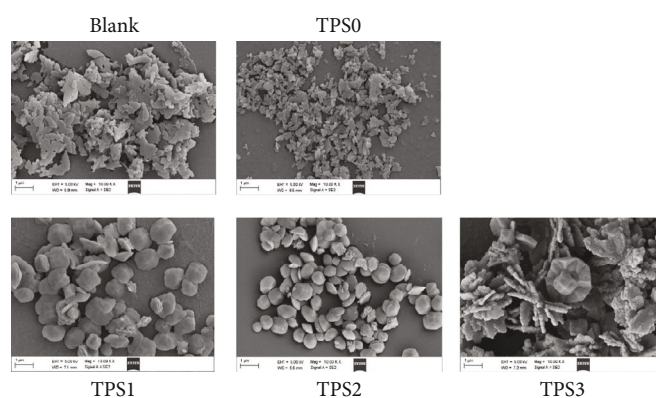
Figure 4 shows that the three degraded TPSs (TPS1, TPS2, and TPS3) can induce COD formation. TPS0 with the largest molecular weight cannot induce COD formation but can reduce the size and aggregation degree of the formed crystals. The percentage of the COD induced by TPS2 with moderate molecular weight was the largest, and the crystal size regulated by TPS2 was the smallest.

3.4. Effect of TPSs with Different Molecular Weights on Inhibition of CaOx Crystal Nucleation and Aggregation.

Figure 5 shows the effect of four TPSs on nucleation and aggregation of the CaOx crystals. After TPSs with different molecular weights were added, the nucleation t_{max} of the crystal was prolonged (Table 3), and the S_N and the crystal S_A of CaOx crystal simultaneously reduced. A total of 0.1 g/L TPS0, TPS1, TPS2, and TPS3 resulted in the

TABLE 2: Infrared characteristic absorption peaks of CaOx crystals formed in the presence of different concentrations of TPSs.

TPSs	c(TPS) (g/L)	COD (%)	$a_{vs}(COO^-)$ (cm^{-1})	$\nu_{as}(COO^-)$ (cm^{-1})	$\nu_s(COO^-)$ (cm^{-1})	COM (cm^{-1})	COD (cm^{-1})	COM (cm^{-1})	COM (cm^{-1})	COM (cm^{-1})	COD (cm^{-1})
Blank	0	0		1617	1325	942		879	781	657	
TPS0	0.1	0		1617	1329	950		878	786	651	
	0.15	0		1618	1329	950		878	786	654	
	0.3	0		1619	1332	953		884	786	655	
	0.5	0		1621	1332	953		883	786	666	
	0.8	0		1627	1334	959		888	792	673	
TPS1	0.1	73	1639		1323		912		786		620
	0.15	84.8	1640		1333		912		786		621
	0.3	100	1645		1334		912				625
	0.5	100	1647		1334		916				625
	0.8	100	1650		1340		917				620
TPS2	0.1	80	1639		1323		917		769		620
	0.15	87	1645		1334		923		780		625
	0.3	100	1646		1337		917				625
	0.5	100	1647		1340		917				616
	0.8	100	1651		1342		918				616
TPS3	0.1	31		1620	1321			885	785	670	618
	0.15	79		1629	1327		912		790		622
	0.3	100	1639		1332		915				616
	0.5	100	1643		1334		916				612
	0.8	100	1646		1335		918				612
COM				1621	1325	947		885	780	663	
COD			1647		1326		916				618

FIGURE 4: SEM images of CaOx crystals regulated by four TPSs. $c(Ca^{2+}) = c(Ox^{2-}) = 10$ mmol/L; $c(TPS) = 0.1$ g/L; crystallization time: 2 h.

nucleation inhibition percentages of 11.12%, 56.67%, 75.52, and 52.92%, and crystal aggregation was inhibited by 7.84%, 22.34%, 47.59%, and 21.59%, respectively. Hence, the inhibition effect of TPSs on crystal nucleation and aggregation followed the order $TPS2 > TPS1 > TPS3 > TPS0$, which indicated that TPS2 with a moderate molecular weight had the best inhibition effect on the nucleation and aggregation of the CaOx crystals.

3.5. Zeta Potential (ζ) of CaOx Crystals with TPSs Having Different Molecular Weights. The changes in ζ of the CaOx crystals generated under the regulation of TPSs with different molecular weights are shown in Figure 6. The ζ values of the crystals without polysaccharide were 1.12 mV. However, the absolute value of ζ in CaOx crystals in the presence of TPSs increased, thereby indicating that the charge density on the crystal surface increased, the repulsive force

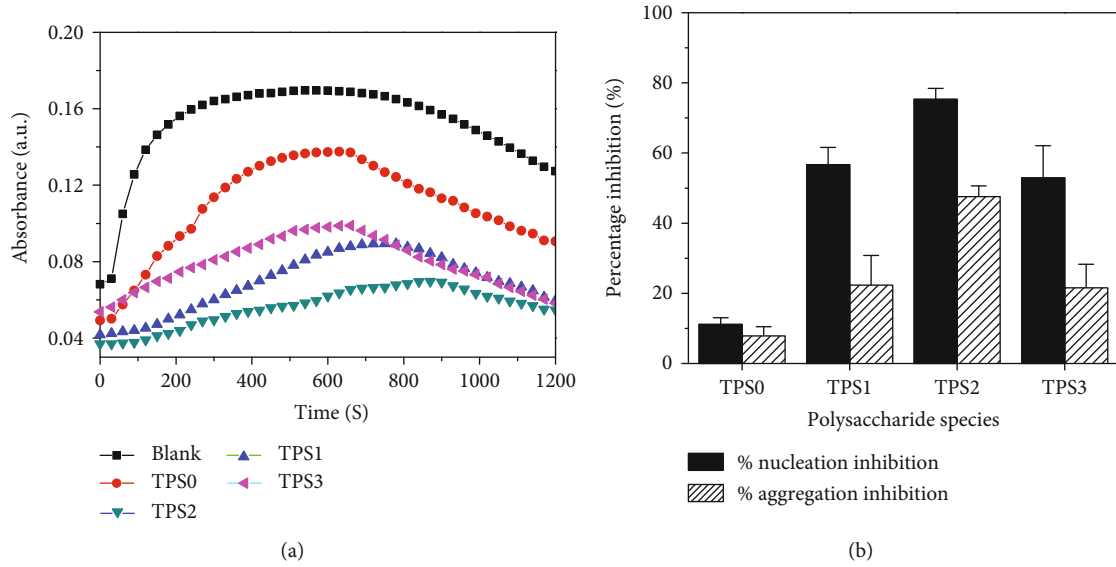


FIGURE 5: (a) Time-course measurements of OD_{620} in five control experiments at standard conditions (4 mmol/L $CaCl_2$ and 0.5 mmol/L Na_2Ox). (b) Percentage inhibition of calcium oxalate crystal nucleation and aggregation by four TPSs with different molecular weights. $c(TPS) = 0.1$ g/L.

TABLE 3: Inhibitory effect of nucleation rate and aggregation rate of CaOx crystals by TPSs.

	Blank	TPS0	TPS1	TPS2	TPS3
t_{max} (s)	540	630	750	840.	660
S_N ($\times 10^{-5}/s$)	17.1 ± 3.12	15.2 ± 3.18	7.41 ± 0.29	4.22 ± 0.98	8.05 ± 0.51
S_A ($\times 10^{-5}/s$)	9.31 ± 1.97	8.58 ± 0.73	7.23 ± 0.91	4.88 ± 0.49	7.3 ± 0.64

Note: t_{max} (s): the moment at which maximum absorbance; S_N : rate of crystal nucleation; S_A : rate of crystal aggregation.

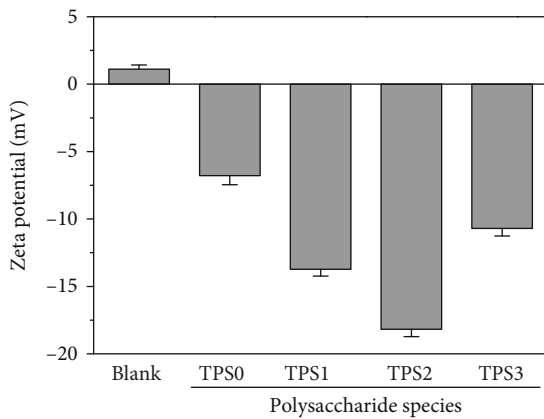


FIGURE 6: Zeta potential of CaOx crystals induced by TPSs with different molecular weights. $c(TPS) = 0.1$ g/L; crystallization time: 2 h.

between crystals increased, and the degree of aggregation between crystals decreased. Given that the absolute ζ value of the crystal was the largest (18.17 mV) in the presence of TPS2, TPS2 had the best performance in inhibiting crystal aggregation.

3.6. Protective Effects of TPSs on HK-2 Cells

3.6.1. Cytotoxicity of TPSs. Given that TPS0 had a weak ability to regulate CaOx crystallization, only TPS1, TPS2, and TPS3 were selected for subsequent cell experiments. TPS1, TPS2, and TPS3 showed no cytotoxicity toward HK-2 cells and had a proliferative effect (100.31%–118.78%, Figure 7(a)).

3.6.2. TPS Protection Increased Antioxidative Damage Ability of HK-2 cells. As shown in Figure 7(b), the cell viability of normal HK-2 cells decreased from 100% to 57.16% after being injured by 2.8 mmol/L oxalic acid. The HK-2 cells were preprotected with TPSs at 20, 40, 60, 80, and 100 μ g/mL for 12 h, and then, 2.8 mmol/L oxalic acid was added. The viability of the cells (75.29%–89.45%) was higher than that of the injured group (57.16%). These results indicated that three TPSs can increase cell resistance to oxidative damage caused by oxalic acid, and the effect was the best when the concentration was 80 μ g/mL.

3.6.3. Release of Lactate Dehydrogenase (LDH) Reduced after Protection by TPSs. LDH is a cytoplasmic enzyme that stably exists in the cytoplasm. When the cell membrane is damaged, LDH is released outside the cell. Therefore, the degree of cell membrane damage can be judged by detecting LDH release.

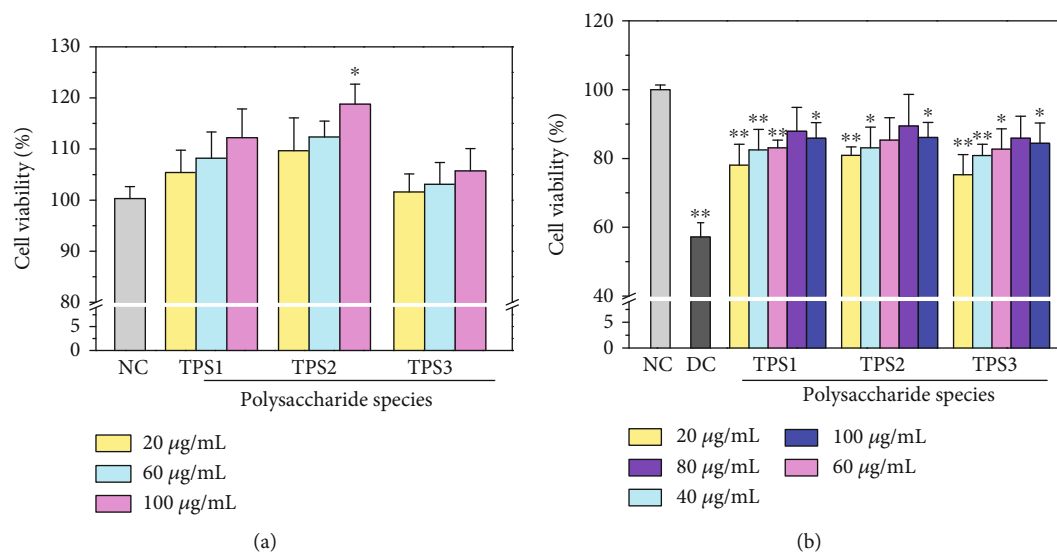


FIGURE 7: (a) Cytotoxicity detection of TPSs with different molecular weights on HK-2 cells. (b) Cell viability changes of HK-2 cell before and after TPSs protection. NC: normal control; DC: damaged control; oxalate damage concentration: 2.8 mmol/L; damage time: 3.5 h; protective time: 12 h.

Figure 8 shows the LDH detection results of normal, injured, and protected cells. Compared with the injured cells, the LDH release of the preprotected cells decreased, thereby indicating that the degree of cell membrane damage decreased, and the protective ability of TPS2 was greater than those of TPS1 and TPS3.

3.6.4. Changes in Cell Morphology after Protection by TPSs. Figure 9 shows the changes in cell morphology before and after TPS protection. The junctions between normal HK-2 cells were tight, and the cells were plump. However, in the injured group, cell density decreased, cell morphology was irregular, and the volume of some cells decreased. After preprotection by TPSs with different molecular weights, the degree of damage of oxalic acid to cell morphology decreased. In particular, the cell morphology of the TPS2 protection group was close to normal cells.

3.6.5. Changes in Intracellular Reactive Oxygen Species (ROS) after Protection by TPSs. Figure 10 shows the changes in the ROS of cells after protecting the three TPSs. The green fluorescence of the cells in the normal group was the weakest (Figure 10(a)), thereby indicating that the ROS level was the lowest. However, ROS was highest in the injured group. After TPS preprotection, the ROS level of the cells was lower than that of the injured group.

Figure 10(b) is a result of quantitative detection of the fluorescence intensity of the ROS generated by cells. Compared with the normal group (2.02%), the fluorescence intensity of the injured cells (37.64%) was the strongest; that is, the ROS level of injured cells was the highest. After being preprotected by TPSs, the fluorescence intensity of the cells decreased at different degrees (16.15%–24.21%, Figure 10(c)). These results indicated that TPSs can reduce ROS generation in cells; that is, TPSs reduced the oxidative

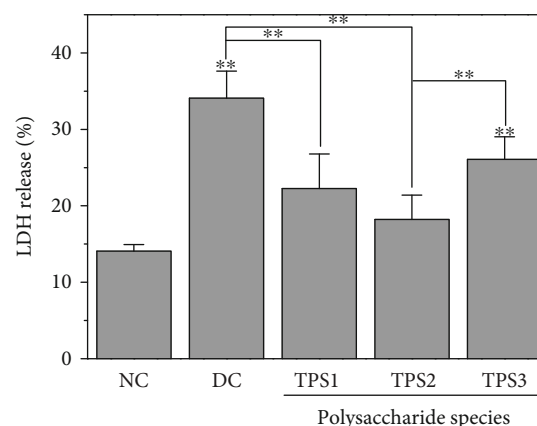


FIGURE 8: LDH release from HK-2 cells before and after TPS protection. $c(\text{TPS}) = 80 \mu\text{g/mL}$. NC: normal control, DC: damaged control; oxalate damage concentration: 2.8 mmol/L; damage time: 3.5 h; protective time: 12 h. Compared with NC group, $*p < 0.05$, $**p < 0.01$.

damage of cells. The degree of reduction was remarkably significant in the TPS2 group (16.15%).

4. Discussion

The formation of kidney stones involves the nucleation, growth, and aggregation of CaOx crystals, as well as the adhesion of crystals to renal epithelial cells. Many acidic molecules in urine, such as citric acid, GAGs, and osteopontin, can inhibit the processes above. TPSs containing abundant $-\text{COOH}$ groups have a chemical structure similar to that of a GAG [26]. Thus, TPSs are potentially effective drugs for inhibiting CaOx kidney stones. This study is aimed at investigating the protective effects of TPSs with different

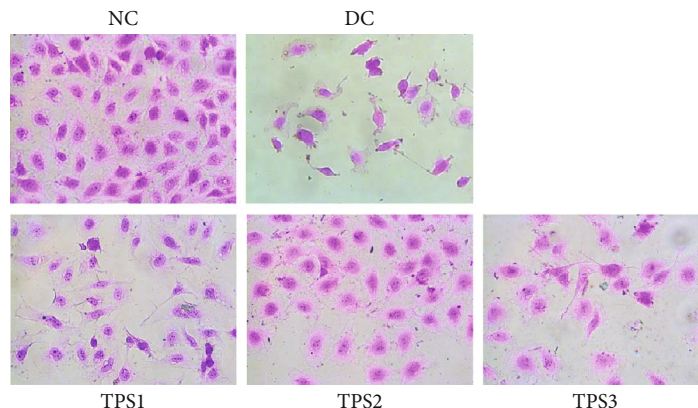


FIGURE 9: Morphological changes of HK-2 cells before and after TPS protection. $c(\text{TPS}) = 80 \mu\text{g/mL}$. The experimental conditions are the same as Figure 8.

molecular weights on HK-2 cells and TPS regulation on CaOx crystallization in vitro (Figure 11).

4.1. TPSs Induced COD Formation. All the FT-IR, XRD, and SEM measurements showed that three degraded TPSs, namely, TPS1, TPS2, and TPS3, can inhibit COM growth and promote COD formation. The induced COD percentage increased with TPS concentration, and TPS2 with a moderate molecular weight had the best effect.

TPSs promote COD formation because TPSs containing acidic groups can adsorb large amounts of Ca^{2+} ions in the solution by electrostatic interaction, which increases the $[\text{Ca}^{2+}]/[\text{Ox}^{2-}]$ ratio in the partial area. Excessive Ca^{2+} ions tend to promote the formation of COD crystals, and excessive Ox^{2-} ions promote the formation of COM crystals [27]. Therefore, COD crystals are easily formed in the presence of TPSs. Given that the polysaccharide surface was enriched with positively charged Ca ions, a high-energy interface was also formed. At the same time, the degree of freedom of the adsorbed Ca ions decreased, and the energy state increased. The high-energy interface and state both promoted the COD formation [28].

Given that the adhesion force between COD crystal and renal cell membrane surface is smaller than COM [29, 30], crystals are relatively easy to be excreted out of the body with urine. Reducing the formation of COM is beneficial to inhibit kidney stone formation. Thus, TPS2 with a moderate molecular weight may have an improved effect on inhibiting urinary stones.

4.2. TPSs Inhibited CaOx Crystal Nucleation and Aggregation. TPSs can effectively inhibit CaOx crystal nucleation and aggregation, and TPS2 had the best effect because when TPSs, which is rich in $-\text{COOH}$ groups, formed soluble complexes with Ca^{2+} ions, the degree of supersaturation of CaOx solution decreased and thereby reduced the S_N of the crystallites. The adsorption of TPSs on crystal caused negative ζ on the crystal surface (Figure 6), thereby increasing the repulsion between the crystals, which inhibited crystal aggregation.

4.3. Degraded TPSs Had Protective Effects on HK-2 Cells. After oxalic acid caused oxidative damage to HK-2 cells, the cell viability decreased (Figure 7), the cell membrane was destroyed, LDH release increased (Figure 8), the cell volume decreased, and tight connections between cells were destroyed (Figure 9). However, the preprotected cells had a strong ability of antioxidative damage. After the cells were injured, excessive ROS was generated by affecting NADPH oxidase activity. ROS accumulation in cells will cause oxidative stress reaction [31]. TPS preprotection can significantly reduce the ROS level of cells (Figure 10), thereby improving the antioxidant capacity of cells.

4.4. Reason for Best Inhibitory Effect of TPS2 with Moderate Molecular Weight. Many factors, such as molecular weight of polysaccharide, acid group content in polysaccharide, glycosidic bond, monosaccharide type, and degree of branching, affect the biological activity of polysaccharide [9], among which molecular weight is one of the most important factors.

- (1) The biological activity of polysaccharide with a large molecular weight decreased. The reason may be due to the following: (a) polysaccharide with an excessive molecular weight has a strong H bond effect and compact structure, which hinders the formation of unfolded structures; (b) polysaccharides have branched chains, large steric hindrance, and large volume [32]; (c) high-molecular-weight polysaccharides exhibit low water solubility, polysaccharide exposed to less active groups in solution than low-molecular-weight polysaccharide, and the interactions between polysaccharides and Ca^{2+} are reduced. Therefore, polysaccharides with an excessive molecular weight cannot effectively inhibit the nucleation and aggregation of crystals and regulate the crystal phase of calcium oxalate. High-molecular-weight polysaccharides feature a large molecular volume which cannot easily cross the cell membrane and enter the cells to exert their biological activity. Sheng and Sun [33] showed that polysaccharides with a low

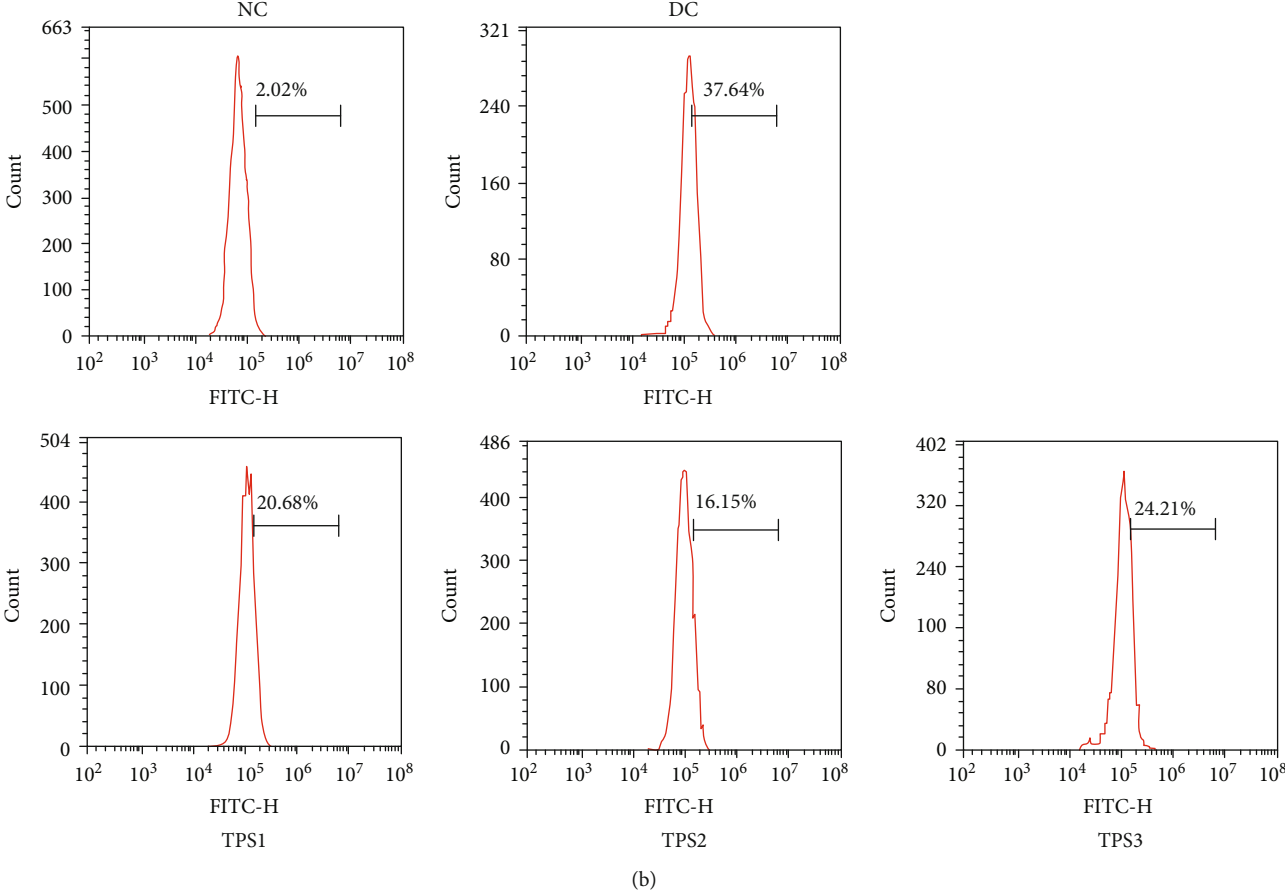
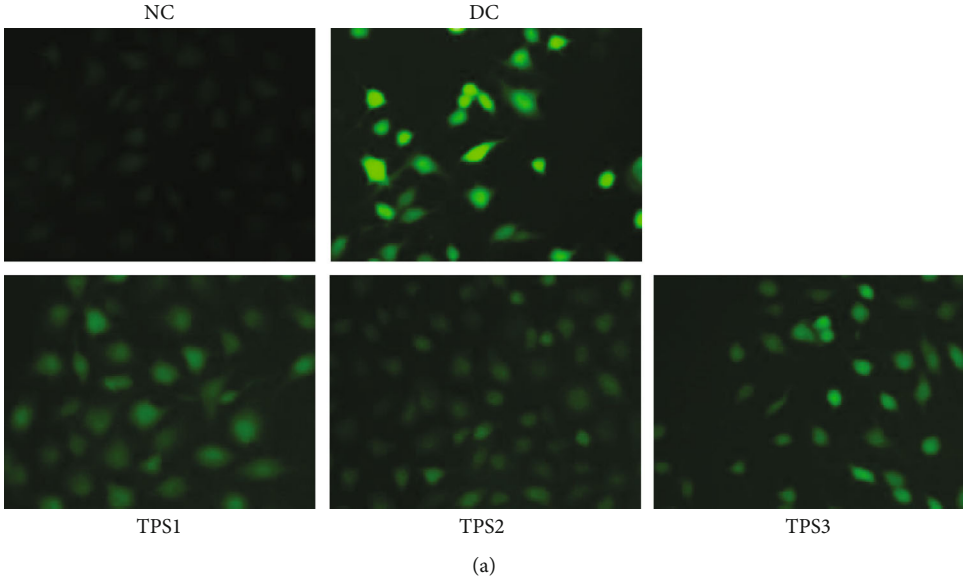
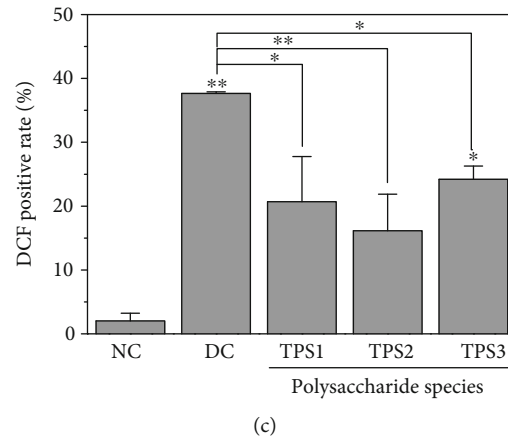


FIGURE 10: Continued.



(c)

FIGURE 10: ROS changes in HK-2 cells before and after TPS protection. (a) Fluorescence microscopy images. (b) Flow cytometry quantitative analysis of fluorescence intensity. (c) Quantitative fluorescence intensity of ROS. $c(\text{TPS}) = 80 \mu\text{g}/\text{mL}$. The experimental conditions and statistical significance are the same as Figure 8.

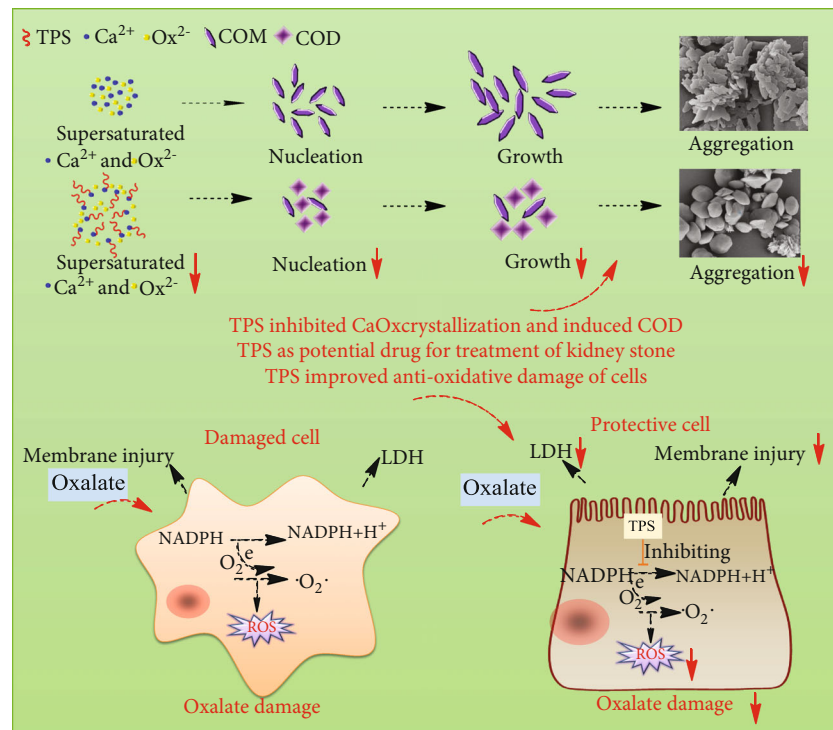


FIGURE 11: Mechanism diagram of TPSs regulating CaOx crystal growth and protecting HK-2 cells from oxidative damage.

molecular weight (1.45–6.4 kDa) have stronger antioxidant activities than those with larger molecular weights (16.89 kDa).

The regulation ability of TPS on CaOx crystals is affected by both its carboxyl group ($-\text{COOH}$) content and molecular weight. TPS2 with a moderate molecular weight and rich in carboxyl group is more conducive to promoting the formation of COD crystals. Although TPS0 (highest MW) and TPS3 (lowest MW) are quite similar with respect to the number of acidic groups they contain (11.2% vs 11.0%), TPS0 did not induce COD formation, while TPS3 induced

31% COD formation. This is because large-molecular-weight polysaccharides have large steric hindrance and less exposed active groups; these factors hinder the interaction between high-molecular-weight TPS0 and Ca^{2+} , resulting in a decrease in the accumulating ability of TPS0 to Ca^{2+} , and it cannot effectively increase the local area $[\text{Ca}^{2+}]/[\text{Ox}^{2-}]$ ratio, so TPS0 did not induce COD formation. Although the number of acidic groups of TPS3 is similar to TPS0, the molecular weight of TPS3 (2.31 kDa) is much smaller than that of TPS0 (10.88 kDa). Therefore, the above factors that hinder the biological activity for TPS0 are obviously reduced for TPS3.

- (2) The biological activity of the polysaccharides with an extremely small molecular weight decreases because polysaccharide with a small molecular weight has a relatively short polysaccharide chain, and the H bond between the polysaccharide chains is weak, which cannot form a complete triple helix polymerization structure with biological activity [34]. The polysaccharide cannot exert its biological activity [35]. For example, Deng et al. [36] showed that the antitumor activity of *Lycium barbarum* polysaccharide with a molecular weight of 40 kDa on mouse liver cancer cells is better than that of 3 kDa
- (3) Only polysaccharide with a moderate molecular weight had the strongest biological activity. Moderate-molecular-weight TPS2 not only had enough space positions to form a complete polymerization structure but also broke the highly compact molecular conformation of the high-molecular-weight polysaccharide and formed unfolded structures, thereby exposing inner functional groups (e.g., $-\text{COOH}$) in polysaccharides. The polysaccharide with a moderate molecular weight has a high degree of freedom and small steric hindrance. The $-\text{COOH}$ content (12.7%) in TPS2 was slightly higher than those of the three other TPSs (11.0%–12.3%).

The factors above are the reasons for the significant increase in the absolute ζ value on the crystal surface that was adsorbed with TPS2 (Figure 6) and increase in the repulsive force between crystals. Given that TPS2 can complex additional Ca^{2+} ions, it has a good inhibiting effect on crystal nucleation and aggregation and can easily enter cells and protect cells from oxidative damage [37]. You et al. [38] showed that *Lentinus edodes* polysaccharides with a moderate molecular weight (306 kDa) has the strongest protective effect on mouse cardiomyocytes against oxidative stress induced by d-galactose compared with those with extremely large (605.0 kDa) and small molecular weights (25.5 kDa).

5. Conclusions

The three degraded TPSs, namely, TPS1, TPS2, and TPS3, have inhibitory effects on the nucleation and aggregation of the CaOx crystals, inhibit COM growth, and induce COD formation. TPSs can protect HK-2 cells from oxidative damage, of which TPS2 with moderate molecular weight has the best effect. Therefore, TPSs, especially TPS2, may prevent the formation of kidney stones.

Data Availability

All the data supporting the results were shown in the paper, and can be applicable from the corresponding author.

Conflicts of Interest

There are no conflicts of interest to declare.

Authors' Contributions

Hong Liu and Xin-Yuan Sun contributed equally to this work.

Acknowledgments

This work was granted by the National Natural Science Foundation of China (Nos. 21975105 and 21701050) and Guangdong Provincial Science and Technology Plan Project (No. 2017B030314108).

References

- [1] A. Bensatal and M. R. Ouahrani, "Inhibition of crystallization of calcium oxalate by the extraction of *Tamarix gallica* L.," *Urological Research*, vol. 36, no. 6, pp. 283–287, 2008.
- [2] D. R. Basavaraj, C. S. Biyani, A. J. Browning, and J. J. Cartledge, "The role of urinary kidney stone inhibitors and promoters in the pathogenesis of calcium containing renal stones," *EAU-EBU Update Series*, vol. 5, no. 3, pp. 126–136, 2007.
- [3] T. Alelign and B. Petros, "Kidney stone disease: an update on current concepts," *Advances in Urology*, vol. 2018, Article ID 3068365, 12 pages, 2018.
- [4] K. P. Aggarwal, S. Narula, M. Kakkar, and C. Tandon, "Nephrolithiasis: molecular mechanism of renal stone formation and the critical role played by modulators," *BioMed Research International*, vol. 2013, Article ID 292953, 21 pages, 2013.
- [5] V. N. Ratkalkar and J. G. Kleinman, "Mechanisms of stone formation," *Clinical Reviews in Bone and Mineral Metabolism*, vol. 9, no. 3–4, pp. 187–197, 2011.
- [6] S. R. Khan, "Reactive oxygen species, inflammation and calcium oxalate nephrolithiasis," *Translational Andrology and Urology*, vol. 3, no. 3, pp. 256–276, 2014.
- [7] N. Xu, Y. Lu, J. Hou, C. Liu, and Y. Sun, "A polysaccharide purified from *Morchella conica* Pers. prevents oxidative stress induced by H_2O_2 in human embryonic kidney (HEK) 293T cells," *International Journal of Molecular Sciences*, vol. 19, no. 12, p. 4027, 2018.
- [8] B. Akin, M. Öner, Y. Bayram, and K. D. Demadis, "Effects of carboxylate-modified, "green" inulin biopolymers on the crystal growth of calcium oxalate," *Crystal Growth & Design*, vol. 8, no. 6, pp. 1997–2005, 2008.
- [9] A. Neira-Carrillo, F. Luengo-Ponce, P. Vásquez-Quitral et al., "Sulfonated polymethylsiloxane as an additive for selective calcium oxalate crystallization," *European Journal of Inorganic Chemistry*, vol. 2015, no. 7, pp. 1167–1177, 2015.
- [10] L. Yang and L. M. Zhang, "Chemical structural and chain conformational characterization of some bioactive polysaccharides isolated from natural sources," *Carbohydrate Polymers*, vol. 76, no. 3, pp. 349–361, 2009.
- [11] M. J. Shi, X. Wei, J. Xu et al., "Carboxymethylated degraded polysaccharides from *Enteromorpha prolifera*: preparation and in vitro antioxidant activity," *Food Chemistry*, vol. 215, pp. 76–83, 2017.
- [12] X. Li, J. Wang, H. Zhang, and Q. Zhang, "Renoprotective effect of low-molecular-weight sulfated polysaccharide from the seaweed *Laminaria japonica* on glycerol-induced acute kidney injury in rats," *International Journal of Biological Macromolecules*, vol. 95, pp. 132–137, 2017.

- [13] C. K. Veena, A. Josephine, S. P. Preetha, P. Varalakshmi, and R. Sundarapandiyam, "Renal peroxidative changes mediated by oxalate: the protective role of fucoidan," *Life Sciences*, vol. 79, no. 19, pp. 1789–1795, 2006.
- [14] J. Xu, M. Wang, J. Zhao, Y. H. Wang, Q. Tang, and I. A. Khan, "Yellow tea (*Camellia sinensis* L.), a promising Chinese tea: processing, chemical constituents and health benefits," *Food Research International*, vol. 107, pp. 567–577, 2018.
- [15] Y. Pan, X. Long, R. Yi, and X. Zhao, "Polyphenols in Liubao tea can prevent CCl₄-induced hepatic damage in mice through its antioxidant capacities," *Nutrients*, vol. 10, no. 9, p. 1280, 2018.
- [16] L. Zhang, Z.-Z. Zhang, Y.-B. Zhou, T.-J. Ling, and X.-C. Wan, "Chinese dark teas: postfermentation, chemistry and biological activities," *Food Research International*, vol. 53, no. 2, pp. 600–607, 2013.
- [17] X. Y. Sun, J. M. Wang, J. M. Ouyang, and L. Kuang, "Antioxidant activities and repair effects on oxidatively damaged HK-2 cells of tea polysaccharides with different molecular weights," *Oxidative Medicine and Cellular Longevity*, vol. 2018, Article ID 5297539, 17 pages, 2018.
- [18] Y. W. Zhao, D. Guo, C. Y. Li, and J. M. Ouyang, "Comparison of the adhesion of calcium oxalate monohydrate to HK-2 cells before and after repair using tea polysaccharides," *International Journal of Nanomedicine*, vol. 14, pp. 4277–4292, 2019.
- [19] L.-S. Huang, X.-Y. Sun, Q. Gui, and J.-M. Ouyang, "Effects of plant polysaccharides with different carboxyl group contents on calcium oxalate crystal growth," *CrystEngComm*, vol. 19, no. 32, pp. 4838–4847, 2017.
- [20] C. Y. Zhang, W. H. Wu, J. Wang, and M. B. Lan, "Antioxidant properties of polysaccharide from the brown seaweed *Sargassum graminifolium* (Turn.), and its effects on calcium oxalate crystallization," *Marine Drugs*, vol. 10, no. 12, pp. 119–130, 2012.
- [21] S. Kulaksizoglu, M. Sofikerim, and C. Cevik, "In vitro effect of lemon and orange juices on calcium oxalate crystallization," *International Urology and Nephrology*, vol. 40, no. 3, pp. 589–594, 2008.
- [22] B. Hess, S. Jordi, L. Zipperle, E. Ettinger, and R. Giovanoli, "Citrate determines calcium oxalate crystallization kinetics and crystal morphology—studies in the presence of Tamm-Horsfall protein of a healthy subject and a severely recurrent calcium stone former," *Nephrology, Dialysis, Transplantation*, vol. 15, no. 3, pp. 366–374, 2000.
- [23] S. Bashir and A. H. Gilani, "Antirolithic effect of *Bergenia ligulata* rhizome: an explanation of the underlying mechanisms," *Ethnopharmacology*, vol. 122, no. 1, pp. 106–116, 2009.
- [24] R. Selvaraju, G. Thirupathi, and A. Raja, "FT-IR spectral studies on certain human urinary stones in the patients of rural area," *Spectrochimica Acta Part A*, vol. 93, no. 10, pp. 260–265, 2012.
- [25] R. C. Walton, J. P. Kavanagh, and B. R. Heywood, "The density and protein content of calcium oxalate crystals precipitated from human urine: a tool to investigate ultrastructure and the fractional volume occupied by organic matrix," *Journal of Structural Biology*, vol. 143, no. 1, pp. 14–23, 2003.
- [26] T. Hattori, K. Kimura, E. Seyrek, and P. L. Dubin, "Binding of bovine serum albumin to heparin determined by turbidimetric titration and frontal analysis continuous capillary electrophoresis," *Analytical Biochemistry*, vol. 295, no. 2, pp. 158–167, 2001.
- [27] T. Jung, W.-S. Kim, and C. K. Choi, "Biom mineralization of calcium oxalate for controlling crystal structure and morphology," *Materials Science and Engineering: C*, vol. 24, no. 1–2, pp. 31–33, 2004.
- [28] J.-M. Ouyang, L. Duan, and B. Tieke, "Effects of carboxylic acids on the crystal growth of calcium oxalate nanoparticles in lecithin–water liposome systems," *Langmuir*, vol. 19, no. 21, pp. 8980–8985, 2003.
- [29] X. Y. Sun, J. M. Ouyang, Y. B. Li, and X. L. Wen, "Mechanism of cytotoxicity of micron/nano calcium oxalate monohydrate and dihydrate crystals on renal epithelial cells," *RSC Advances*, vol. 5, no. 56, pp. 45393–45406, 2015.
- [30] X. Sheng, M. D. Ward, and J. A. Wesson, "Crystal surface adhesion explains the pathological activity of calcium oxalate hydrates in kidney stone formation," *Journal of the American Society of Nephrology*, vol. 16, no. 7, pp. 1904–1908, 2005.
- [31] Y. Chen, L. Ye, W. Li, D. Li, and F. Li, "Hyperoside protects human kidney-2 cells against oxidative damage induced by oxalic acid," *Molecular Medicine Reports*, vol. 18, no. 1, pp. 486–494, 2018.
- [32] M. Jiangwei, Q. Zengyong, and X. Xia, "Optimisation of extraction procedure for black fungus polysaccharides and effect of the polysaccharides on blood lipid and myocardium antioxidant enzymes activities," *Carbohydrate Polymers*, vol. 84, no. 3, pp. 1061–1068, 2011.
- [33] J. Sheng and Y. Sun, "Antioxidant properties of different molecular weight polysaccharides from *Athyrium multidentatum* (döll.) Ching," *Carbohydrate Polymers*, vol. 108, pp. 41–45, 2014.
- [34] H. Saitô, Y. Yoshioka, N. Uehara, J. Aketagawa, S. Tanaka, and Y. Shibata, "Relationship between conformation and biological response for (1→3)- β -d-glucans in the activation of coagulation Factor G from limulus amoebocyte lysate and host-mediated antitumor activity. Demonstration of single-helix conformation as a stimulant," *Carbohydrate research*, vol. 217, no. 1, pp. 181–190, 1991.
- [35] K. I. Berker, B. Demirata, and R. Apak, "Determination of total antioxidant capacity of lipophilic and hydrophilic antioxidants in the same solution by using ferric-ferricyanide assay," *Food Analytical Methods*, vol. 5, no. 5, pp. 1150–1158, 2012.
- [36] X. Deng, X. Li, S. Luo, Y. Zheng, X. Luo, and L. Zhou, "Antitumor activity of *Lycium barbarum* polysaccharides with different molecular weights: an *in vitro* and *in vivo* study," *Food & Nutrition Research*, vol. 61, no. 1, p. 1399770, 2017.
- [37] Z. Xu, X. Li, S. Feng et al., "Characteristics and bioactivities of different molecular weight polysaccharides from camellia seed cake," *International Journal of Biological Macromolecules*, vol. 91, pp. 1025–1032, 2016.
- [38] R. You, K. Wang, J. Liu, M. Liu, L. Luo, and Y. Zhang, "A comparison study between different molecular weight polysaccharides derived from *Lentinus edodes* and their antioxidant activities *in vivo*," *Pharmaceutical Biology*, vol. 49, no. 12, pp. 1298–1305, 2011.